spinons might bind with a finite binding energy—it appears that this might be happening on cylinder YC10 and, thus, it might also occur in the 2D limit. For the even cylinders, on the other hand, the spinons are confined by an effective potential that grows linearly with the distance, because the domain between them is in the higher-energy sector. As a result, the excitation across the spin gap for the even cylinders is a bound spinon pair. It remains to be determined if they remain bound in the 2D limit.

Much remains to be understood concerning the low-energy behavior of the KHA, particularly the detailed structure, exchange statistics, and dispersion relations of the various excitations. It will be instructive to also explore the phase diagram in the vicinity of this simple nearest-neighbor–only Heisenberg model by changing the Hamiltonian in various ways (*13*) to find what other phases are nearby and perhaps to move "deeper" into this spin liquid where it might be easier to study.

References and Notes
1. V. Elser, *Phys. Rev. Lett.* **62**, 2405 (1989).
2. J. B. Marston, C. Zeng, *J. Appl. Phys.* **69**, 5962 (1991).
3. S. Sachdev, *Phys. Rev. B* **45**, 12377 (1992).
4. L. Balents, *Nature* **464**, 199 (2010).
5. S. R. White, *Phys. Rev. Lett.* **69**, 2863 (1992).
6. S. R. White, *Phys. Rev. B* **48**, 10345 (1993).
7. P. Nikolic, T. Senthil, *Phys. Rev. B* **68**, 214415 (2003).
8. R. R. P. Singh, D. A. Huse, *Phys. Rev. B* **76**, 180407 (2007).
9. R. R. P. Singh, D. A. Huse, *Phys. Rev. B* **77**, 144415 (2008).
10. G. Evenbly, G. Vidal, *Phys. Rev. Lett.* **104**, 187203 (2010).
11. D. Poilblanc, M. Mambrini, D. Schwandt, *Phys. Rev. B* **81**, 180402(R) (2010).
12. H. C. Jiang, Z. Y. Weng, D. N. Sheng, *Phys. Rev. Lett.* **101**, 117203 (2008).
13. P. Sindzingre, C. Lhuillier, *Europhys. Lett.* **88**, 27009 (2009).
14. Y. Ran, M. Hermele, P. A. Lee, X.-G. Wen, *Phys. Rev. Lett.* **98**, 117205 (2007).
15. Supporting material is available on *Science* Online.
16. P. W. Leung, V. Elser, *Phys. Rev. B* **47**, 5459 (1993).
17. A. M. Läuchli, J. Sudan, E. S. Sørensen, http://arxiv.org/abs/1103.1159.
18. P. W. Anderson, *Mater. Res. Bull.* **8**, 153 (1973).
19. S. A. Kivelson, D. S. Rokhsar, J. P. Sethna, *Phys. Rev. B* **35**, 8865 (1987).
20. N. Read, B. Chakraborty, *Phys. Rev. B* **40**, 7133 (1989).
21. N. Read, S. Sachdev, *Phys. Rev. Lett.* **66**, 1773 (1991).
22. X. G. Wen, *Phys. Rev. B* **44**, 2664 (1991).
23. R. Moessner, S. L. Sondhi, *Phys. Rev. Lett.* **86**, 1881 (2001).
24. G. Misguich, D. Serban, V. Pasquier, *Phys. Rev. B* **67**, 214413 (2003).
25. E. Lieb, T. Schultz, D. Mattis, *Ann. Phys.* **16**, 407 (1961).
26. C. Waldtmann *et al.*, *Eur. Phys. J. B* **2**, 501 (1998).

Two-Dimensional Mott-Hubbard Electrons in an Artificial Honeycomb Lattice

A. Singha,[1]* M. Gibertini,[1] B. Karmakar,[1] S. Yuan,[2] M. Polini,[1,3]† G. Vignale,[4,3] M. I. Katsnelson,[2] A. Pinczuk,[5] L. N. Pfeiffer,[6] K. W. West,[6] V. Pellegrini[1]†

Artificial crystal lattices can be used to tune repulsive Coulomb interactions between electrons. We trapped electrons, confined as a two-dimensional gas in a gallium arsenide quantum well, in a nanofabricated lattice with honeycomb geometry. We probed the excitation spectrum in a magnetic field, identifying collective modes that emerged from the Coulomb interaction in the artificial lattice, as predicted by the Mott-Hubbard model. These observations allow us to determine the Hubbard gap and suggest the existence of a Coulomb-driven ground state.

The conduction electrons of a crystal experience the potential created by a periodic arrangement of coupled quantum units (such as ions and atoms). Numerous properties of solids can be explained in terms of Bloch bands (*1*), neglecting Coulomb interactions between electrons. These interactions often lead to qualitative changes that are particularly pronounced in solids with narrow energy bands (*2–4*). These strongly correlated materials display exotic ordering phenomena and metal-insulator phase transitions (*3*, *4*). Mott showed (*5*) that interaction-induced insulators are better described in real space (rather than in momentum space), in which the solid is viewed as a collection of localized electrons bound to atoms with partially filled shells. Electrons hopping through the lattice are absorbed and emitted from the atoms, thus originating two bands, which are split by the energy cost of having two electrons with antiparallel spin on the same atomic site.

Hubbard subsequently introduced a model Hamiltonian with onsite interactions that displays split bands (Hubbard bands, or HBs) in the strongly correlated (or atomic) limit (*6*). HBs (and their coexistence with quasiparticle bands in the correlated metallic phase) are characteristic features of such strongly correlated systems. Fermions on a honeycomb lattice, in particular, have been predicted to display unusual correlated phases of matter such as topological Mott insulating (*7*) and quantum spin liquid phases (*8*).

The creation of artificial systems with a high degree of tunability offers a way to explore Mott-Hubbard (M-H) physics systematically

(*9*, *10*). Here we report the creation of an artificial lattice with honeycomb geometry for trapping electrons, and we demonstrate the formation of HBs through strong correlations. We nanofabricated the artificial lattice on the surface of a gallium arsenide (GaAs) heterostructure that hosts a high-quality two-dimensional electron gas (2DEG) (*11–13*). Similar nanostructures have been studied in the past in the context of the Hofstadter's fractal energy spectrum (*14*, *15*). We probed the electron excitation spectrum by inelastic light-scattering and observed signatures stemming from strong Coulomb interactions, which we could tune by applying an external magnetic field. Carriers in the patterned structures supported an unusual collective mode; its energy scales like $\sqrt{B}$, where B is the component of the magnetic field perpendicular to the 2DEG. A theoretical analysis based on a minimal Hubbard model reveals that the mode energy is determined by the onsite Coulomb interaction and represents direct evidence of the existence of HBs in the 2DEG subjected to the artificial lattice. At low temperatures and large B fields, we found evidence for the opening of an unexpected gap in the spin excitation spectrum. We argue that the observed gap reveals the occurrence of a new correlated phase of electrons in a honeycomb lattice akin to one of those discussed in the context of graphene in high magnetic fields (*16–18*). These findings pave the way for the possibility to explore graphene-like physics in the ultrahigh magnetic field limit, in which the magnetic length is smaller than the lattice constant of the artificial crystal—a regime not accessible in graphene.

The sample used in this study was the host of a 2DEG in a 25-nm-wide, one-side modulation-doped $Al_{0.1}Ga_{0.9}As$/GaAs quantum well. The procedures for nanofabricating the artificial lattice are detailed in (*11*, *19*, *20*). The artificial honeycomb lattice extended over a 100-μm–by–100-μm

[1]National Enterprise for nanoScience and nanoTechnology, Istituto Nanoscienze–CNR, and Scuola Normale Superiore, I-56126 Pisa, Italy. [2]Radboud University Nijmegen, Institute for Molecules and Materials, NL-6525 AJ Nijmegen, Netherlands. [3]Kavli Institute for Theoretical Physics China, Chinese Academy of Sciences, Beijing 100190, China. [4]Department of Physics and Astronomy, University of Missouri, Columbia, MO 65211, USA. [5]Department of Applied Physics and Applied Mathematics and Department of Physics, Columbia University, New York, NY, USA. [6]Department of Electrical Engineering, Princeton University, Princeton, NJ, USA.

*Present address: Department of Physics, Bose Institute, 93/1 Acharya Prafulla Chandra Road, Kolkata 700009, India.
†To whom correspondence should be addressed. E-mail: vp@sns.it (V.P.); m.polini@sns.it (M.P.)

square region with a lattice constant $a \sim 130$ nm (Fig. 1A). We denote by V_0 the amplitude of the artificial lattice potential. Here we focus on a sample with an estimated (12) $V_0 \sim 4$ meV and electron density after processing $n_e \sim 3 \times 10^{10}$ to 4×10^{10} cm^{-2} corresponding to an average number of eight electrons per site. The inelastic light-scattering experiments were performed in a backscattering configuration (Fig. 1B) in the temperature range from 50 mK to 4 K. The light-scattering technique gives direct access to the collective modes of the system that manifest as sharp peaks in the intensity of the scattered light

at a given energy shift from the laser energy. Resonant enhancement of the light-scattering cross section occurs as the incident laser energy is scanned across an interband transition of the host GaAs semiconductor (20).

The nanostructured 2DEG displays well-resolved quantum Hall signatures below 3 T, with the honeycomb potential manifesting itself in a modulation of the magnetoresistivity periodic in B (12). At higher fields, an increase in the longitudinal resistivity signals a crossover to a regime of suppressed intersite hopping in which collective modes emerge.
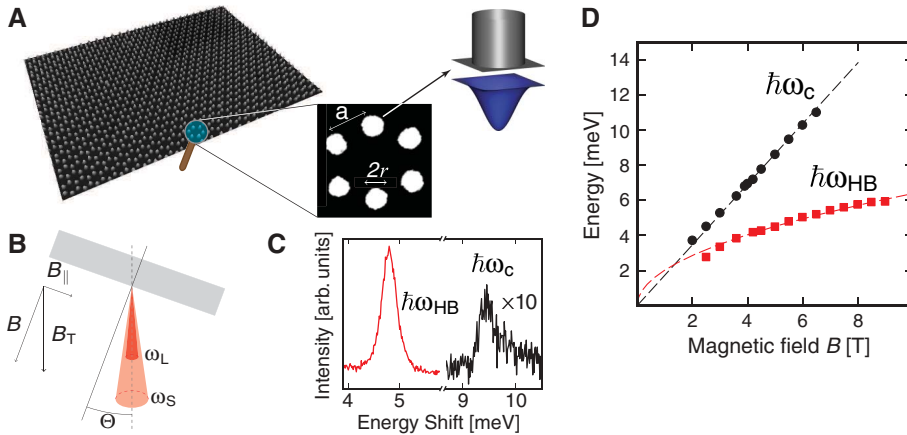
In addition to the ordinary cyclotron mode (black curve in Fig. 1C and black circles in Fig. 1D) at energy $\hbar\omega_c = \hbar eB/(m^*c)$, m^* being the GaAs electron effective mass (21), the light-scattering spectra display an additional mode at lower energies (red curve in Fig. 1C), whose collective character is reflected in the sharpness and intensity of the light-scattering peak (22, 23). The surprising sublinear dependence of the energy of this mode on B is shown in Fig. 1D (red squares).

We identified the sublinear collective mode as a Hubbard mode: an excitation across split HBs. In the simplest scenario, this excitation emerges within the single-band Hubbard model (3, 4, 6) that assumes a maximum concentration of two electrons per site. We proceeded by first evaluating the M-H excitation gap as a function of B and then showing that it weakly depends on electron concentration, consistent with the experimental data presented below. Similar conclusions can be reached by using multiband generalizations of the Hubbard model (20).

The single-band Hubbard Hamiltonian encodes a competition between two energy scales: the kinetic energy t, which measures the overlap between electronic wave functions on neighboring lattice sites, and the interaction energy U, which measures the strength of the onsite Coulomb repulsion between two electrons

$$H = -t \sum_{\langle i,j \rangle} c_i^+ c_j + \varepsilon_0 \sum_i n_i + U \sum_i n_{i\uparrow} n_{i\downarrow} \quad (1)$$

Here the operator c_i^+ (c_i) creates (destroys) an electron at site i (the sum in the first term is over all pairs of nearest-neighbor sites), and $n_i = c_i^+ c_i$ is the local number operator; ε_0 denotes the energy of the single state that is available at each site i: This can be either empty, singly, or doubly occupied. In writing Eq. 1, we have neglected first-neighbor (intersite) interactions. In the atomic, strongly correlated limit $U \gg t$, two split HBs emerge out of a single narrow band (6). More precisely, this means that for $U \gg t$, the spectral function (that is, the tunneling density of states $A(\omega)$ of the model described by Eq. 1) develops two peaks, one at $\hbar\omega = \varepsilon_0$ and one at $\hbar\omega = \varepsilon_0 + U$. The emergence of HBs when the ratio U/t increases from the weakly to the strongly correlated regime is accurately described by dynamical mean-field theory (2–4).

In the experiments, the strongly correlated regime $U \gg t$ is achieved when B quenches the hopping amplitude t and increases the interaction energy U. The Hubbard-U interaction scale can be written in terms of localized Wannier functions $\Phi(r)$ as

$$U = \int d^2\mathbf{r} \int d^2\mathbf{r}' |\phi(\mathbf{r})|^2 V_{ee}(|\mathbf{r} - \mathbf{r}'|) |\phi(\mathbf{r}')|^2 \quad (2)$$

where $V_{ee}(r) = e^2/(\varepsilon r)$ is the long-range Coulomb interaction, with ε an effective dielectric constant. In the atomic limit, the Wannier functions can be roughly approximated by a zero–angular-

Fig. 1. (**A**) Scanning electron microscopy (SEM) image of the semiconductor artificial lattice. An expanded view of the SEM image showing a single honeycomb cell ($2r \sim 60$ nm, $a \sim 130$ nm) is shown at middle right. The 2DEG is positioned 170 nm below the surface with a low-temperature mobility of 2.7×10^6 cm^2/(Vs). A cartoon of the two-dimensional potential trap for electrons induced by the nanofabricated pillar at the surface is shown at far right (arrow). (**B**) Geometry of the light-scattering experiment: $\omega_{L,s}$ labels the incident (scattered) photon energy and $\Theta = 5°$ is the tilt angle. (**C**) Resonant inelastic light-scattering spectra showing the cyclotron mode and the new low-lying collective mode at $B = 5.48$ T and $T = 1.7$ K. (**D**) Evolution of the energies of the cyclotron mode (black circles) and of the new collective mode at frequencies ω_{HB} (red squares) at $T = 1.7$ K. The black dashed line is a linear fit to the data using $\hbar\omega_c = \hbar eB/(m^*c)$. We find $m^* = 0.067\ m_e$ with m_e the bare electron mass, in agreement with the bulk GaAs value. The red dashed line is a fit with $\hbar\omega_{HB} = \alpha\sqrt{B[T]}$ and $\alpha \sim 2$ meV.
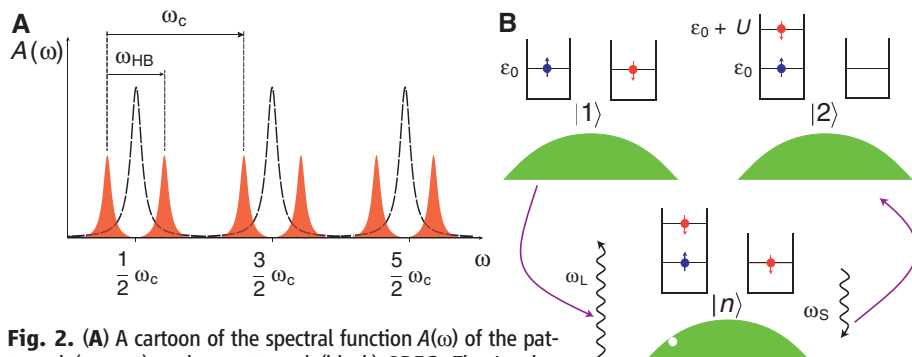

Fig. 2. (**A**) A cartoon of the spectral function $A(\omega)$ of the patterned (orange) and unpatterned (black) 2DEG. The Landau level peaks at $\omega_n = \omega_c(n + 1/2)$ are split by onsite Coulomb interactions into Hubbard lower and upper peaks, which are separated by $U \sim e^2/l_B$, where $l_B = \sqrt{\hbar c/eB}$ is the magnetic length. (**B**) The relevant electronic process that contributes to the Raman scattering cross section. The initial state is labeled by $|1\rangle$, the final state by $|2\rangle$, and the intermediate state with one hole and an extra electron is labeled by $|n\rangle$. The final excited state is separated from the ground state by the Hubbard charge gap U; that is, by the energy cost of having two antiparallel spin electrons on the same site. In the intermediate state, we have also depicted the absorbed (at frequency ω_L) and emitted (at frequency ω_S) photons. The square wells denote two neighboring minima of the artificial-lattice potential. The core levels are not shown. The green areas denote valence-band electrons, which are assumed to be unaffected by the periodic modulation.

momentum wavefunction in the symmetric gauge, $\phi(\mathbf{r}) = (2\pi l_B^2)^{-1/2} \exp[-r^2/(4l_B^2)]$, where $l_B = \sqrt{\hbar c/eB}$ is the magnetic length. Simple algebraic manipulations on Eq. 2 yield

$$U = \sqrt{\frac{\pi}{4}} \frac{e^2}{\varepsilon l_B} \qquad (3)$$

implying that, at least asymptotically, U grows proportionally to $\sqrt{B}$. Microscopic details such as the precise shape of the confinement potential or the geometry of the lattice might affect the result in Eq. 3 quantitatively but not qualitatively: The scaling $\propto \sqrt{B}$ is robust in the asymptotic limit $l_B \ll 2r$, where $2r$ is the width of the potential minima of the artificial lattice (Fig. 1A).

The function $A(\omega)$ in a B field is pictorially illustrated in red in Fig. 2A. As a comparison, the black dashed line labels $A(\omega)$ for an unpatterned 2DEG: We distinguish the usual Landau-level peaks at frequencies $\omega_n = \omega_c(n + 1/2)$ with integer n. In the nanopatterned sample, these peaks are split into upper and lower Hubbard peaks by strong interactions. In this cartoon, the measured cyclotron mode at $\omega_c \propto B$ is an inter–Landau-level excitation. The measured sublinear mode seen in Fig. 1, instead, can be neatly explained as an intra–Landau-level excitation, which lies at a frequency $\omega_{HB} = U/\hbar \propto \sqrt{B}$, between interaction-induced Hubbard peaks (24, 25).

After fitting the data labeled by red squares in Fig. 1D with the simple functional form $\hbar\omega_{HB} = \alpha\sqrt{B[\text{T}]}$, we found that α was ~2 meV, thereby providing a direct measurement of the Hubbard-U onsite energy scale for our nanopatterned 2DEG. The measured U is by a factor of 2 smaller than the value extracted from Eq. 3 with the high-frequency GaAs dielectric constant $\varepsilon = 13$. In Fig. 2B, we illustrate a possible two-photon process that contributes to the scattering cross section of the HB collective mode. The calculated scattering cross section decays exponentially for sufficiently large values of B (20). In Fig. 3 we report the resonant inelastic light-scattering spectra of the Hubbard mode as a function of external parameters. Figure 3A shows that, in contrast to the cyclotron mode, the intensity of the Hubbard mode increased up to $B \approx 5.5$ T and then collapsed exponentially at higher fields, in agreement with the theoretical prediction.

The Hubbard mode energy exhibited a rather weak dependence on electron concentration (Fig. 3B); we decreased the electron concentration using a photodepletion technique (20). In the atomic limit, the dependence of the M-H gap $\hbar\omega_{HB}$ on electron concentration is indeed a small effect, of the first order in the parameter t/U. In the limit of vanishing electron concentration, the strength of the transition between the two HBs also vanishes because there are no available states in the upper HB (20). This finding is in agreement with the large dependence of the intensity of the Hubbard mode on electron density reported in Fig. 3B. Finally, the Hubbard mode displays a large sensitivity to temperature changes (Fig. 3C) and disappears near 5 K.

We now focus on the low-energy portion of the excitation spectra, $\hbar\omega < 1$ meV, which in ordinary 2DEGs is characterized by the spin-wave (SW) mode—a spin-flip excitation across the spin gap that, at long wavelength, occurs at the bare Zeeman energy $g\mu_B B_T$, where μ_B is the Bohr magneton, g is the Landé gyromagnetic factor, and $B_T = \sqrt{B_\parallel^2 + B^2}$ is the total magnetic field (Fig. 1B). The inset to Fig. 4 shows a representative result at $B_T = 5.5$ T. The SW mode was visible at energies near 0.15 meV. The SW energy versus total field is reported in Fig. 4 as black circles. The spin mode was not visible below $B_T = 3$ T.

The inset to Fig. 4 displays an additional strong and sharp mode above the SW, which has no counterpart in an unpatterned 2DEG. The energy dependence of this mode is shown in Fig. 4 as red triangles. The splitting Δ of this mode from the SW (black squares) occurs above a

threshold B value and depends on the perpendicular magnetic field only, a fact that underlines the pivotal role of electron-electron interactions. The two modes disappear at temperatures approaching 1 K. The observation of a spin doublet suggests the occurrence of a correlated state with a gap Δ. Different types of Coulomb-driven broken-symmetry scenarios have been proposed in the context of graphene at large magnetic fields (26–31) and linked to observations of gap openings in magneto-transport experiments (16–18). One of these scenarios (28) predicts a splitting of the SW mode similar to what we saw in our experiment (32) associated to the occurrence of lattice-scale order in the honeycomb lattice.

In the case of graphene, however, the high-field regime is not experimentally accessible, because the magnetic length is much greater than the interatomic distance. This is not the case in our artificial honeycomb lattice. To support the existence of graphene-like effects in our system,
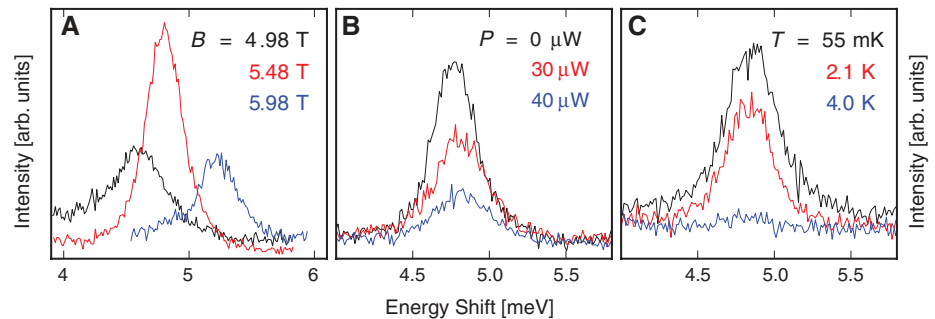

Fig. 3. (A) Resonant inelastic light-scattering spectra of the Hubbard mode at three values of the magnetic field and $T = 1.7$ K. **(B)** Dependence of the Hubbard mode at $T = 1.5$ K on the power P (in microwatts) of the HeNe laser used to photodeplete the 2DEG. From black to blue, the electron concentration per site decreases from 8 ± 2 to 3 ± 2 (21). Data in (A) are at $P = 0$ μW. **(C)** Temperature dependence of the Hubbard mode at $B = 5.48$ T and $P = 0$ μW, displaying an activated behavior with an activation energy of 0.2 meV.

Fig. 4. Energies of the spin-wave mode (black circles) and the higher-energy spin-flip mode (red triangles). The black dashed line is a linear fit to the data using the standard Zeeman formula: $E_{SW} = |g|\mu_B B_T$. We find $|g| = 0.42$, in agreement with the value expected for GaAs. Representative examples of the two spin excitation modes at two different laser energies (red line, 1522.6 meV; black line, 1522.4 meV) are shown in the inset. The black squares label the splitting Δ between the two spin modes.
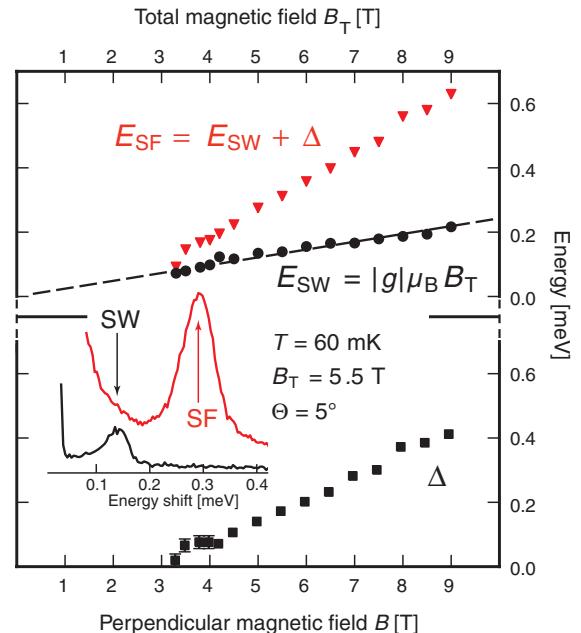
we carried out calculations of the density of states based on a tight-binding model (33) in the presence of disorder comparable to the hopping energy and in the ultrahigh–magnetic-field regime ($l_B < a$). These results reveal the persistence of a structure reminiscent of the zero-energy Landau level of graphene (20). Similar to the case in graphene (16–18, 31), electron-electron interactions can lead to a reorganization of this low-energy sector, yielding a broken-symmetry ground state with an energy gap ~ Δ. Additionally, the observed opening of the gap above a threshold magnetic field indicates a delicate interplay between hopping, disorder, and many-body effects.

The capability of observing M-H physics in nanostructured semiconductor devices with honeycomb geometry may open new approaches for the investigation of quantum phases of strongly correlated condensed-matter systems. Given that the interaction strengths governing the physics of the 2DEG can be finely tuned by design and by the application of external electric and magnetic fields, such scalable solid-state systems offer great promise to further expand the current realms of study offered by quantum emulators that so far have been realized with cold atom gases in optical lattices (34–36).

References and Notes

1. N. W. Ashcroft, N. D. Mermin, *Solid State Physics* (Saunders College, Philadelphia, PA, 1976).
2. G. Kotliar, D. Vollhardt, *Phys. Today* **57**, 53 (2004).
3. G. Kotliar et al., *Rev. Mod. Phys.* **78**, 865 (2006).
4. D. Vollhardt, A. Avella, F. Mancini, *AIP Conf. Proc.* **1297**, 339 (2010).
5. N. F. Mott, *Proc. Phys. Soc. (London) A* **62**, 416 (1949).
6. J. Hubbard, *Proc. Roy. Soc. (London) A* **281**, 401 (1964).
7. S. Raghu, X.-L. Qi, C. Honerkamp, S.-C. Zhang, *Phys. Rev. Lett.* **100**, 156401 (2008).
8. Z. Y. Meng, T. C. Lang, S. Wessel, F. F. Assaad, A. Muramatsu, *Nature* **464**, 847 (2010).
9. I. Buluta, F. Nori, *Science* **326**, 108 (2009).
10. T. Byrnes, N. Y. Kim, K. Kusudo, Y. Yamamoto, *Phys. Rev. B* **78**, 075320 (2008).
11. M. Gibertini, A. Singha, V. Pellegrini, M. Polini, G. Vignale, A. Pinczuk, L. N. Pfeiffer, K. W. West, *Phys. Rev. B* **79**, 241406(R) (2009).
12. G. De Simoni et al., *Appl. Phys. Lett.* **97**, 132113 (2010).
13. C.-H. Park, S. G. Louie, *Nano Lett.* **9**, 1793 (2009).
14. C. Albrecht et al., *Phys. Rev. Lett.* **86**, 147 (2001).
15. S. Melinte et al., *Phys. Rev. Lett.* **92**, 036802 (2004).
16. Y. Zhang et al., *Phys. Rev. Lett.* **96**, 136806 (2006).
17. J. G. Checkelsky, L. Li, N. P. Ong, *Phys. Rev. Lett.* **100**, 206801 (2008).
18. A. J. M. Giesbers et al., *Phys. Rev. B* **80**, 201403 (2009).
19. C. P. García et al., *Phys. Rev. Lett.* **95**, 266806 (2005).
20. See supporting material on *Science* Online.
21. A. Pinczuk et al., *Phys. Rev. Lett.* **68**, 3623 (1992).
22. For example, intra-dot excitations probed in arrays of isolated quantum dots display broad (several milli–electron volts) and weak transitions (23).
23. S. Kalliakos et al., *Nat. Phys.* **4**, 467 (2008).
24. Inelastic light-scattering does not directly probe $A(\omega)$ but the density-density dynamical structure factor $S(\omega)$. The latter function contains, in general, extra excitations with respect to the former: These are of two-particle nature and stem from vertex corrections (25). In the single-band Hubbard model, though, these effects are of minor relevance. In this model and in the strongly correlated regime, a double-peaked spectral function implies a resonance in $S(\omega)$ at a frequency $\omega_{HB} = U/\hbar$.
25. M. I. Katsnelson, A. I. Lichtenstein, *J. Phys. Condens. Matter* **22**, 382201 (2010).
26. K. Nomura, A. H. MacDonald, *Phys. Rev. Lett.* **96**, 256602 (2006).
27. D. A. Abanin, P. A. Lee, L. S. Levitov, *Phys. Rev. Lett.* **96**, 176803 (2006).
28. J. Alicea, M. P. A. Fisher, *Phys. Rev. B* **74**, 075422 (2006).
29. V. P. Gusynin, V. A. Miransky, S. G. Sharapov, I. A. Shovkovy, *Phys. Rev. B* **74**, 195429 (2006).
30. For a recent review, see, for example, (36).
31. D. S. L. Abergel, V. Apalkov, J. Berashevich, K. Ziegler, T. Chakraborty, *Adv. Phys.* **59**, 261 (2010).
32. In our experiment, in which the electron density [and not the filling factor (28)] was fixed, the splitting should increase with $\sqrt{B}$, as in the case of the mode at $\hbar\omega_{HB}$ discussed above. This is, however, not consistent with the experimental data in Fig. 4, probably due to the relevance of disorder at low energies.
33. S. Yuan, H. De Raedt, M. I. Katsnelson, *Phys. Rev. B* **82**, 115448 (2010).
34. M. Greiner, O. Mandel, T. Esslinger, T. W. Hänsch, I. Bloch, *Nature* **415**, 39 (2002).
35. M. Lewenstein et al., *Adv. Phys.* **56**, 243 (2007).
36. I. Bloch, J. Dalibard, W. Zwerger, *Rev. Mod. Phys.* **80**, 885 (2008).

A Material with Electrically Tunable Strength and Flow Stress

Hai-Jun Jin[1,2]* and Jörg Weissmüller[3,4]

The selection of a structural material requires a compromise between strength and ductility. The material properties will then be set by the choice of alloy composition and microstructure during synthesis and processing, although the requirements may change during service life. Materials design strategies that allow for a recoverable tuning of the mechanical properties would thus be desirable, either in response to external control signals or in the form of a spontaneous adaptation, for instance in self-healing. We have designed a material that has a hybrid nanostructure consisting of a strong metal backbone that is interpenetrated by an electrolyte as the second component. By polarizing the internal interface via an applied electric potential, we accomplish fast and repeatable tuning of yield strength, flow stress, and ductility. The concept allows the user to select, for instance, a soft and ductile state for processing and a high-strength state for service as a structural material.

Environmental exposure and in-service wear influence the mechanical performance of engineering materials. Environmental effects are often adverse, as exemplified by stress corrosion cracking (1). Immersion in corrosive media may also impair strength and flow stress without immediate failure (2–4). More recently, nanoindentation studies have revealed a decisive effect of the surface state on the hardness (5). Although the microscopic processes that couple the plasticity to the environment have not been conclusively determined, the observations demonstrate that a material's mechanical performance can vary depending on the environment to which it is exposed during service. Here, we exploit these observations in designing a material with controllable strength and ductility. Our approach rests on two principles. First, we maximize the impact of surface processes by working with nanomaterials with an extremely large surface area. Second, we design the material as a hybrid in which an electrolyte becomes an inherent part of the microstructure. Interfacial properties and processes can be controlled via an electric potential, with consequences for the macroscopic behavior of the nanocomposite. In this way, the yield strength and flow stress of our material can be recoverably varied by as much as a factor of 2.

Our samples are made by dealloying, a corrosion process that selectively dissolves the less noble component from an alloy and leaves behind a monolithic body with a uniform, nanometer-scale structure composed of a contiguous skeleton of "ligaments" of the more noble component interpenetrated by an equally contiguous pore

[1]Shenyang National Laboratory for Materials Science, Institute of Metal Research, Chinese Academy of Sciences, 110016 Shenyang, P.R. China. [2]Institute of Nanotechnology, Karlsruhe Institute of Technology, D-76021 Karlsruhe, Germany. [3]Institut für Werkstoffphysik und -Technologie, Technische Universität Hamburg-Harburg, D-21073 Hamburg, Germany. [4]Institut für Werkstoffphysik, Werkstoffmechanik, Helmholtz Zentrum Geesthacht, D-21502 Geesthacht, Germany.

*To whom correspondence should be addressed. E-mail: hjjin@imr.ac.cn